Electronic Supplementary Information:

Chirality as a tool for function in porous organic cages

T. Hasell,[a*] M. A. Little,[a] S. Y. Chong,[a] M. Schmidtmann,[a] M. E. Briggs,[a] V. Santolini,[b] K. E. Jelfs,[b] and A. I. Cooper[a*]

Department of Chemistry and Center for Materials Discovery, University of Liverpool, Crown St., Liverpool L69 7ZD, UK

KEYWORDS: Porous organic cages; microporous; chiral separation; cocrystal; polymorph, crystal engineering.

Note on Helicity:

Helicity, or axial chirality, is an intrinsic property of the monomeric cages. All six bisimino vertices must be of the same enantiomer, and the vertex substituents must occupy exo-positions to facilitate a tetrahedral molecular structure. This means that even if a racemic mixture of *R* and *S* diamines is used to synthesise cages, each cage molecule itself will still be chiral, although the resultant mixture of *R* and *S* cages will of course be racemic. In the case of **CC3**, the homochiral diamine starting material is readily available. As such **CC3** is regularly produced in our group in its chiral form, **CC3**-*R* or **CC3**-*S*. However, it can also be produced from the racemic diamine, which produces a racemic mixture of *R* and *S* cages, which then co-crystallise in an alternating structure. Both homochiral and racemic **CC3** crystallise in the window-to-window diamondoid pore structure. The diamines used to produce **CC1** and **CC13** are not chiral themselves. However, the resulting cages are chiral – and of a racemic mixture of *R* and *S* helical chirality that co-crystallise. The diamine used to produce **CC2** (i.e. 1,2-diaminopropane) is a chiral molecule – but the racemic mixture is used normally to produce the cage. The resultant **CC2** is therefore also a mixture of *R* and *S* cages which also co-crystallise together. However, the use of the chiral diamine (*R*-1,2-diaminopropane, or *S*-1,2-diaminopropane, both available as hydrochloride salts), produces the resultant chiral cage (**CC2**-*R* or **CC2**-*S*).

Methods:

Materials: 1,3,5-Triformylbenzene (TFB) was purchased from Manchester Organics, UK and used as received. 2-Methyl-1,2-propanediamine was purchased from TCI Europe and used as received. All other chemicals were purchased from Sigma-Aldrich and used as received.

Synthesis: **CC1**, **CC2**(racemic), **CC3**, and **CC13** were all made as previously described.[1-4] Chiral **CC2** was synthesized as follows: TFB (1.46 g, 9.01 mmol) was dissolved in acetonitrile (600 mL) in a1 L round bottom flask, under continuous stirring and cooled by an ice bath. To this was added dropwise, by pressure equalizing dropping funnel, a solution of (*R*)-1,2-diaminopropane dihydrochloride (2 g, 13.6 mmol) and triethylamine (2.75 g) in an equal volume mixture of acetonitrile and methanol (300 mL). The resultant mixture was left stirring under nitrogen for 24 hours before the solution was rotary evaporated (at 20 °C) to dryness. The resultant white powdery solid was triturated with tetrahydrofuran (200 mL) and filtered to remove the triethylamine-HCl salt. The filtrate was again evaporated down to yield the pure product as a white powder (1.73 g, 88% yield).

HPLC separation: Purification of the **CC2**-*S*/**CC3**-*R* cocrystal was carried out on a Shimadzu Prominence Preparative HPLC equipped with a Syncronis C8 column (97205-159370, 150 x

30 mm, 5 µm) using a flow rate of 40 mL/min of methanol for 12 min. The **CC2-***R* containing fractions were concentrated at 10 °C on a rotary evaporator.

Single Crystal Data: Single crystal X-ray data sets were measured at beamline I19, Diamond Light Source, UK using silicon double crystal monochromated synchrotron radiation (λ = 0.6889 Å),[5] or on a Rigaku MicroMax-007 HF rotating anode diffractometer (Mo-Kα radiation, λ = 0.71073 Å, Kappa 4-circle goniometer, Rigaku Saturn724+ detector). Empirical absorption corrections, using equivalent reflections, were applied by the program SADABS.[6] Structures were solved by SHELXD or SHELXS,[7] and refined by full-matrix least squares on $|F|^2$ by SHELXL,[7] interfaced through the programme OLEX2.[8] Unless started, all non H-atoms were refined anisotropically, and unless stated H-atoms were fixed in geometrically estimated positions and refined using the riding model. Absolute configurations were not determined crystallography. Supplementary single crystal XRD data files, including structure factors, are available free of charge from the Cambridge Crystallographic Data Centre (CCDC) via www.ccdc.cam.ac.uk/data_request/cif.

Crystal data for **CC2**-*R*·1.7(*para*-xylene) crystallized from a CH_2Cl_2 *para*-xylene solution, CCDC number 1520508: Formula $C_{67.59}H_{76.99}N_{12}$; M = 1057.51 g·mol^{-1}; orthorhombic space group $P2_12_12_1$, colourless needle shaped crystal; a = 11.1553(19) Å, b = 19.490(4) Å, c = 30.332(6) Å; V = 6595(2) Å^3; ρ = 1.065 g·cm^{-3}; μ(synchrotron λ = 0.6889 Å) = 0.061 mm^{-3}; F (000) = 2266; crystal size = 0.21 × 0.07 × 0.05 mm; T = 100(2) K; 34167 reflections measured (1.649 < θ < 22.501°), 9431 unique (R_{int} = 0.0507), 7494 ($I > 2\sigma(I)$); R_1 = 0.0786 for observed and R_1 = 0.0948 for all reflections; wR_2 = 0.2297 for all reflections; max/min difference electron density = 0.537 and -0.313 e·Å^{-3}; data/restraints/parameters = 9431/76/749; GOF = 1.084. Flack parameter 0.2(10).

Crystal data for **CC2**-*R*·4.5(1,4-dioxane)·4.25(H_2O) crystallized from a CH_2Cl_2 1,4-dioxane solution, CCDC number 1520510: Formula $C_{130}H_{160.5}N_{24}O_{15.25}$; M = 2303.31 g·mol^{-1}; cubic space group $P2_13$, colourless crystal; a = 24.318(2) Å; V = 14381(4) Å^3; ρ = 1.064 g·cm^{-3}; μ(synchrotron λ = 0.6889 Å) = 0.066 mm^{-3}; F (000) = 4922; crystal size = 0.15 × 0.10 × 0.05 mm; T = 100(2) K; 45501 reflections measured (1.148 < θ < 22.517°), 6914 unique (R_{int} = 0.0772), 5558 ($I > 2\sigma(I)$); R_1 = 0.0722 for observed and R_1 = 0.0860 for all reflections; wR_2 = 0.2134 for all reflections; max/min difference electron density = 0.363 and -0.273 e·Å^{-3}; data/restraints/parameters = 6914/48/609; GOF = 1.047. Flack parameter 0.3(10).

Crystal data for **CC3**-*R*·**CC13**-*R*6(2-propanol)·CH_2Cl_2·4(H_2O) crystallized from a CH_2Cl_2 2-propanol solution. CCDC 1520509: Formula $C_{151}H_{214}Cl_2N_{24}O_{10}$; M = 2596.35 g·mol^{-1}; hexagonal space group $P6_3$, colourless hexagonal shaped crystal; a = 17.5938(7) Å, c = 32.2344(13) Å; V = 8641.1(8) Å^3; ρ = 0.998 g·cm^{-3}; μ(Mo-Kα) = 0.093 mm^{-3}; F (000) = 2804; crystal size = 0.24 × 0.20 × 0.08 mm; T = 100(2) K; 37680 reflections measured (1.336 < θ < 23.255°), 7633 unique (R_{int} = 0.0532), 6186 ($I > 2\sigma(I)$); R_1 = 0.0916 for observed and R_1 = 0.1121 for all reflections; wR_2 = 0.2709 for all reflections; max/min difference electron density = 0.587 and -0.337 e·Å^{-3}; data/restraints/parameters = 7633/74/595; GOF = 1.078. Flack parameter 0.84(10).

Crystal data for **CC3**-*R*·0.65(**CC13**-*S*)·0.35(**CC13**-*R*)·1.96(1,4-dioxane)·2.25(CH_2Cl_2)·6(H_2O) crystallized from a CH_2Cl_2 1,4-dioxane solution; CCDC 1520511: Formula $C_{142.09}H_{188.18}Cl_{5.50}N_{24}O_{9.92}$; M = 2586.19 g·mol^{-1}; trigonal space group $P321$, colourless plate shaped crystal; a = 17.5575(7) Å, c = 28.6921(12) Å; V = 7659.8(7) Å^3; ρ = 1.121 g·cm^{-3}; μ(Mo-Kα) = 0.164 mm^{-3}; F (000) = 2763; crystal size = 0.16 × 0.15 × 0.03 mm; T = 100(2) K; 53335 reflections measured (0.710 < θ < 21.966°), 6254 unique (R_{int} = 0.0948), 5557 (I >

$2\sigma(I)$); R_1 = 0.1285 for observed and R_1 = 0.1435 for all reflections; wR_2 = 0.3421 for all reflections; max/min difference electron density = 0.713 and -0.686 e·Å^{-3}; data/restraints/parameters = 6254/230/595; GOF = 2.359. Flack parameter 0.69(8).

Powder X-ray Diffraction: Laboratory powder X-ray diffraction (PXRD) data were collected in transmission mode on loose powder samples held on thin Mylar film in aluminium well plates on a Panalytical X'Pert PRO MPD equipped with a high throughput screening (HTS) XYZ stage, X-ray focusing mirror and PIXcel detector, using Cu Kα radiation. Data were measured over the range 4–50° in ~0.013° steps over 60 minutes. High resolution synchrotron PXRD were collected for a sample of the (**CC2**-*S*/**CC3**-*R*) cocrystal contained in a 0.7 mm borosilicate glass capillary at beamline I11 at Diamond Light Source, using the Mythen-II position sensitive (λ = 0.827153 Å). A capillary spinner was used to improve powder averaging. Indexing, Le Bail fitting and Rietveld refinement were performed using *TOPAS-Academic* version 5.[9] Rietveld refinement of (**CC2**-*S*/**CC3**-*R*) required geometric restraints on all bond lengths and angles, which were derived from the corresponding solvated single crystal structure.

Gas Sorption Analysis: Surface areas were measured by nitrogen adsorption and desorption at 77.3 K. Powder samples were degassed offline at 100 °C for 15 h under dynamic vacuum (10^{-5} bar) before analysis, followed by degassing on the analysis port under vacuum, also at 100 °C. Isotherms were measured using Micromeritics 2020, or 2420 volumetric adsorption analyzer.

Scanning Electron Microscopy. Imaging of the crystal morphology was achieved using a Hitachi S-4800 cold Field Emission Scanning Electron Microscope (FE-SEM). Samples were prepared by depositing dry crystals on 15 mm Hitachi M4 aluminum stubs using an adhesive high purity carbon tab before coating with a 2 nm layer of gold using an Emitech K550X automated sputter coater. Imaging was conducted at a working distance of 8 mm and a working voltage of 3 kV using a mix of upper and lower secondary electron detectors.

Co-crystallisation of CC3/CC13: 500 mg of **CC3** dissolved in 40 mL DCM was mixed with 861 mg **CC13** in dissolved in 10 mL DCM. The resultant solution was left in an open vessel in a tank of acetone (or 1,4 dioxane) for 7 days. Filtering then yielded 835 mg of white powder (90% of the ideal yield if all **CC3** and half **CC13** had precipitated out). NMR confirms that the precipitate is close to a 1:1 ratio of **CC3**:**CC13** (1:0.97), and that the filtrate is almost entirely **CC13**.

NMR: Solution ^{1}H NMR spectra were recorded at 400.13 MHz using a Bruker Avance 400 NMR spectrometer. Variable temperature NMR was conducted using the standard Bruker VT unit using a liquid N_2 heat exchanger with the temperature regulated with a thermocouple. The cage/CD_2Cl_2 solution was cooled in steps and allowed to equilibrate for 20 minutes prior to data acquisition. Data analysis was performed using OriginPro8.0 graphical software. The simulated spectra were generated using the WINDMNR-Pro software (H.J. Reich, h ttp://www.chem.wisc.edu/areas/reich/plt/windnmr.htm).

Computational methods:

Four porous organic cages (**CC1**, **CC2**, **CC3**, and **CC13**) were investigated, starting from their *R* enantiomer. In order to energetically study the chiral interconversion mechanism from the *R* enantiomer to the *S* enantiomer, each cage was modified according to the following interconversion steps. The mechanism involves the two main factors, the flip of the C-C=N-C torsions, and the movement of the bulky steric groups from the *exo* to *endo* position. All the steps involved were investigated both individually and combined to try to understand why CC2 and **CC3** cannot interconvert, and why **CC1** and **CC13** can. A representation of the processes involved is shown in Figure S12. Figure S12-A show the initial cage (CC2 in the example) in the *R* enantiomer. Next, Figure S12-B shows the movement of all the bulky groups from the *exo* to the *endo* position only, Figure S12-C the flipping of the C-C=N-C torsions only, and Figure S12-D a combination of both the torsion flipping and the methyl groups movement. Table S1 reports the modifications that were applied to each cage to understand how much energy it could approximately cost to start the chiral interconversion. At the beginning of the study only one torsion was flipped per cage, and only one bulky group was moved for **CC2** and **CC3**. A further investigation involving the flipping of all the torsions was performed on **CC2** and **CC3**, whereas a simulation including both the flipping and the movement of the bulky groups from *exo* to *endo* was performed on **CC2** only.

Each structure was initially analysed with a 1 ns molecular dynamics simulation performed with the Macromodel Software (Schrödinger PLC – version 2016-3) and with the recently released OPLS3 force field.[10] The forcefield was previously used to investigate the energetics and geometry of porous organic cages with successful results.[11] The simulation was conducted at 300 K with a time step of 1.5 fs, and 500 structures were sampled and minimised. This was to locate the local minima to the initial guess that was hand constructed. In order to refine the structures' geometry and their energies, each cage was then optimised with density functional theory (DFT) using NWChem,[12] with the Minnesota M06-2X functional,[13] combined with a 6-31G* standard Pople basis set. All the relative energies were calculated with respect to the cages in their *R*-enantiomer, and are shown in Figure 13. **CC1** and **CC13** are destabilised by the initial flipping of one C-C=N-C torsion, as their energy is respectively raised by 12.9 and 16.7 kJ mol^{-1}. Similarly **CC2** and **CC3** are destabilised by respectively 21.5 and 19.4 kJ mol^{-1}. For the last two molecules, just moving one bulky group into the *endo* position without flipping a torsion is not as destabilising and the energies of both are only raised by 7.5 and 7.7 kJ mol^{-1}. Combining the movement into *endo* with the flip just moves the energies of the two cages to respectively 22.9 and 21.9 kJ mol^{-1}.

A more thorough investigation was then performed on **CC2**. Results show how moving all the methyl groups into the *endo* position destabilises the molecule by 45.6 kJ mol^{-1}. Flipping all the torsions greatly strained the structure raising its energy by 135.5 kJ mol^{-1}. In order to reduce the strain and go back to a more stable conformation the molecule would need to move the methyl groups from the *exo* to *endo* position. The combination of this last step combined to the flipping shows that the molecule is actually stabilised and that its energy decreases by more than 86 kJ mol^{-1}. It was not possible to conduct the same study on **CC3** as the cyclohexane group prevents the exo-to-endo movement. However, it was possible to study the effect of flipping the C-C=N-C torsions, simulating the interconversion toward the *S* enantiomer. **CC3** is also destabilised by the strain of flipping all the C-C=N-C torsions and its energy moves up to 136.5 kJ mol^{-1}. The exchange of the chirality around the arene group without the

corresponding movement of the bridging vertices leads to an extremely high energy cost that and an extremely strained conformation. The movement of the bulky groups to the *endo* position releases the strain but therefore leads to a less favourable arrangement than the opposite chirality *exo* structure.

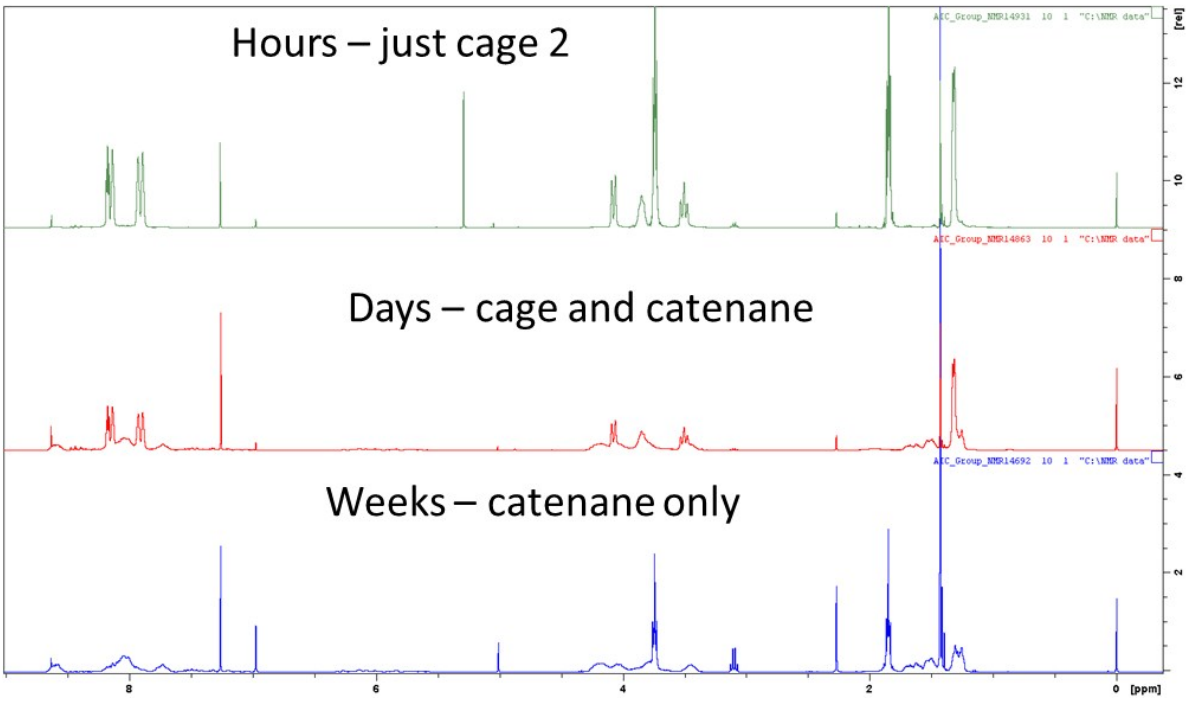

Figure S1: NMR of homochiral **CC2** synthesis (aliquots taken directly from the synthesis), showing rapid formation of catenanes.

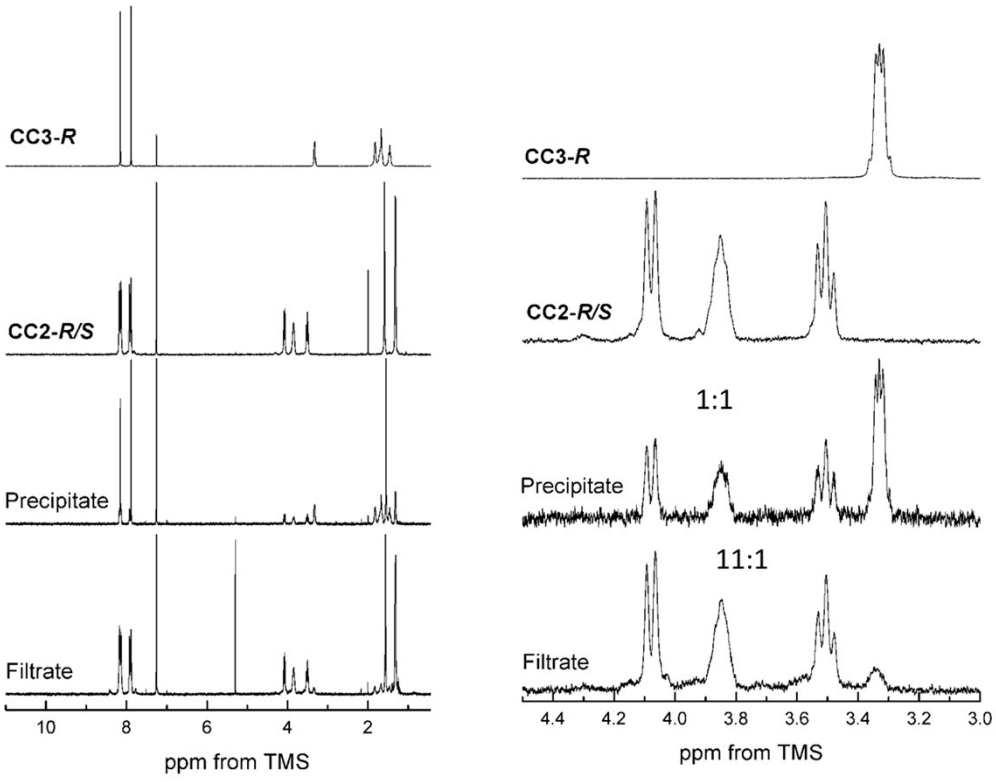

Figure S2: NMR of **CC2** separation by co-crystallisation, and close up of the region compared by integration. This gave a **CC2**:**CC3** ratio of 1:1 in the cocrystal precipitate, and 11:1 in the filtrate.

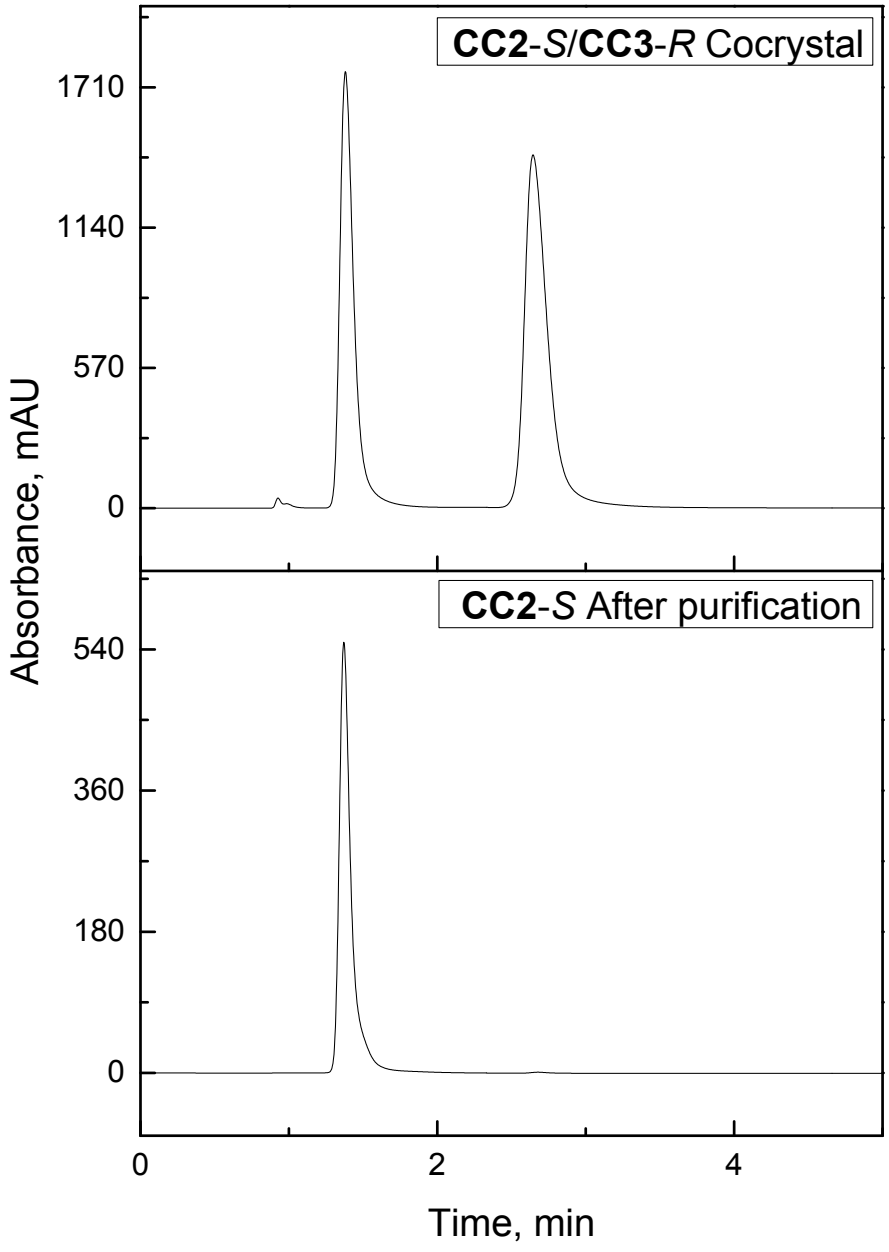

Figure S3: Figure showing HPLC spectra for the **CC2**-*S*/**CC3**-*R* cocrystal, and **CC2**-*S* after purification (Dionex Ultimate 3000; ThermoScientific Hypersil GOLD Phenyl column (25903-152136, 150 x 2.1 mm, 3 μm); 0.5 mL/min isocratic methanol for 5 min; 254 nm.

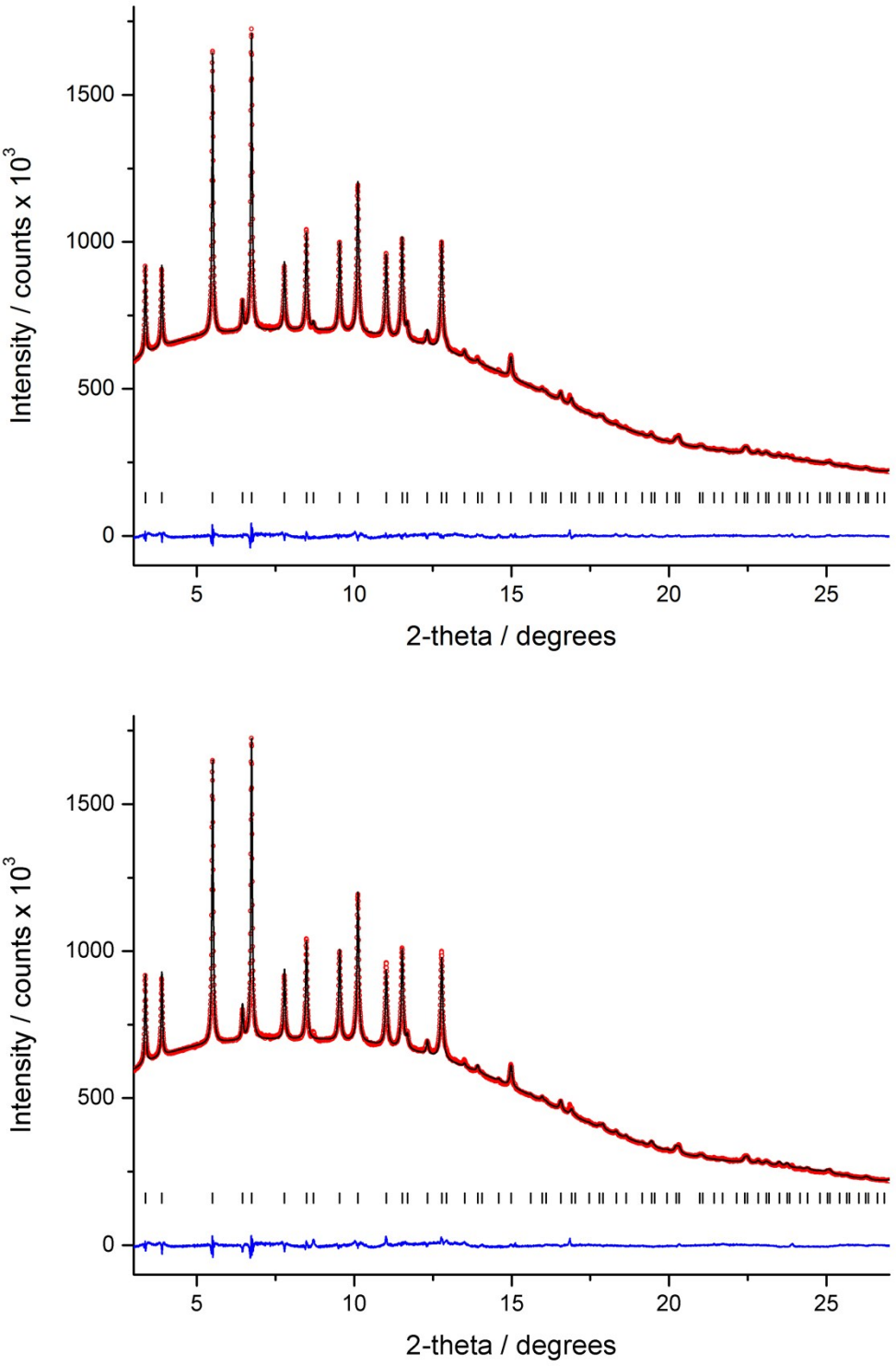

Figure S4:. Final Le Bail (*top*; a = 24.3679(4) Å, V = 14469.5(6) Å^3, $F23$; R_{wp} = 1.69 %, R_p = 1.53 %, χ^2 = 4.98) and Rietveld (*bottom*; R_{wp} = 1.69 %, R_p = 1.53 %, χ^2 = 5.76 R_{Bragg} = 2.55 %; 138 reflections, 63 parameters, 39 geometric restraints) refinements for **CC2**-*S*/**CC3**-*R* cocrystal (a = 24.3768(4) Å, V = 14469.3(6) Å^3, $F23$). Observed (red points), calculated (black line) and difference (blue line) profiles are shown and reflection positions are also indicated below.

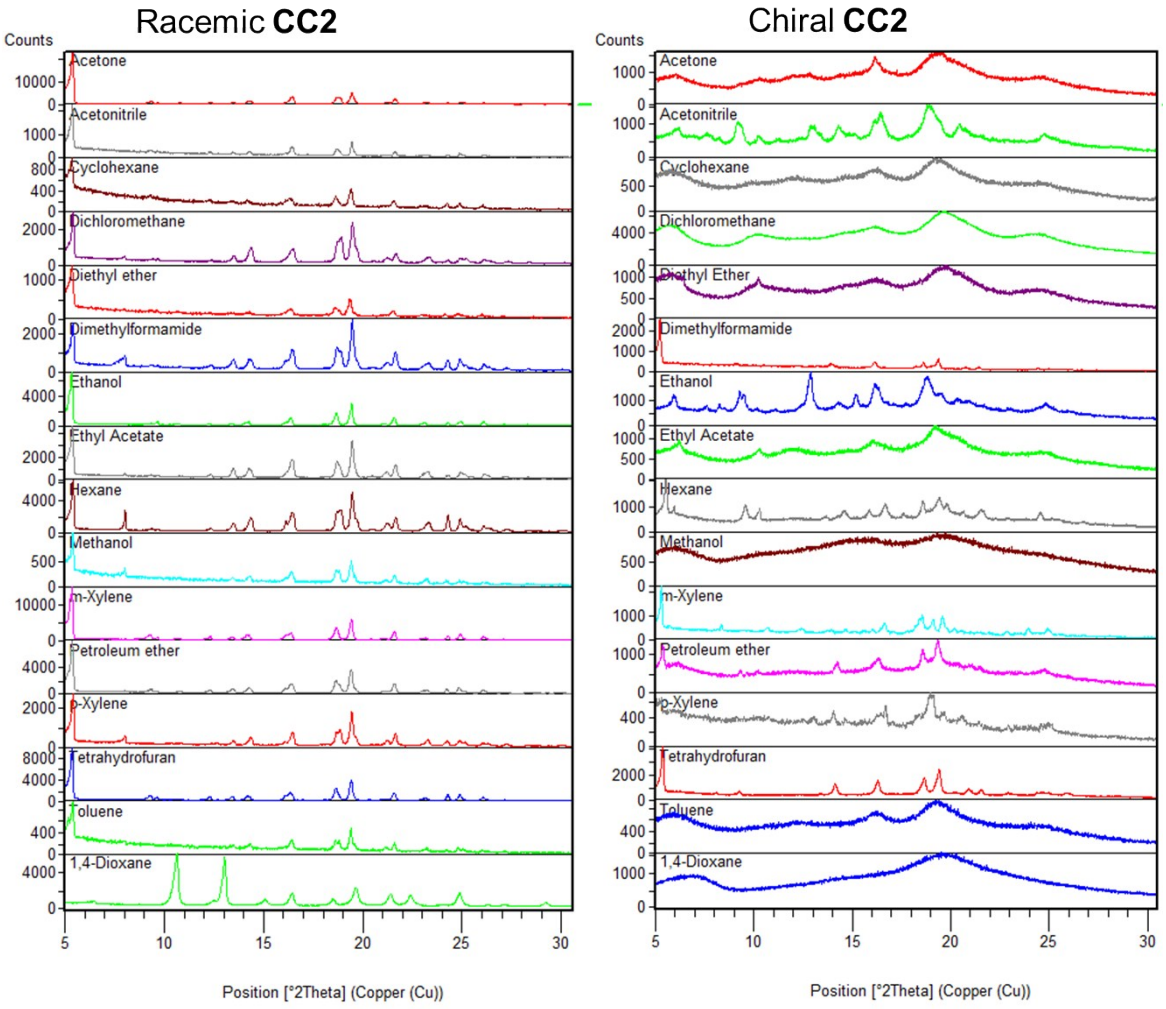

Figure S5: PXRD patterns of racemic **CC2** (left) and homochiral **CC2** (right). All samples were dissolved in dichloromethane, before crystals were grown by solvent diffusion/evaporation with the co-solvent listed. The produced crystals were dried of solvent before PXRD. It can be observed that racemic **CC2** forms a crystalline phase from all solvents tested, whereas homochiral **CC2** is regularly amorphous. All solvents tested with racemic **CC2** gave the α phase (with 1-D channels), except for 1,4-dioxane which gives a window-to-window packing β phase that is related to the packing of **CC3**α. In the case of chiral **CC2**, 1,4-dioxane gives an alternative polymorph as the solvate, but this is not stable to desolvation and becomes amorphous.

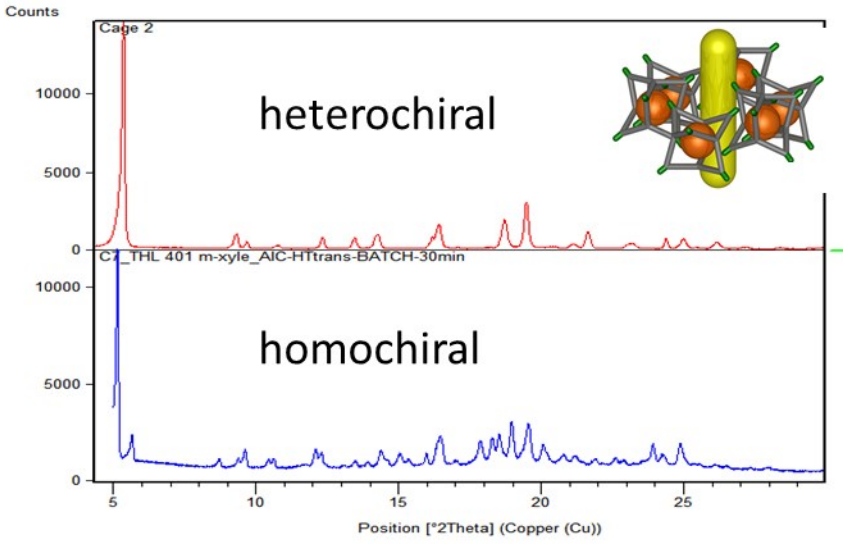

Figure S6: PXRD patterns of racemic **CC2**α with one dimensional pore channels, compared to the desolvated form of chiral **CC2** crystallized with *m*-xylene.

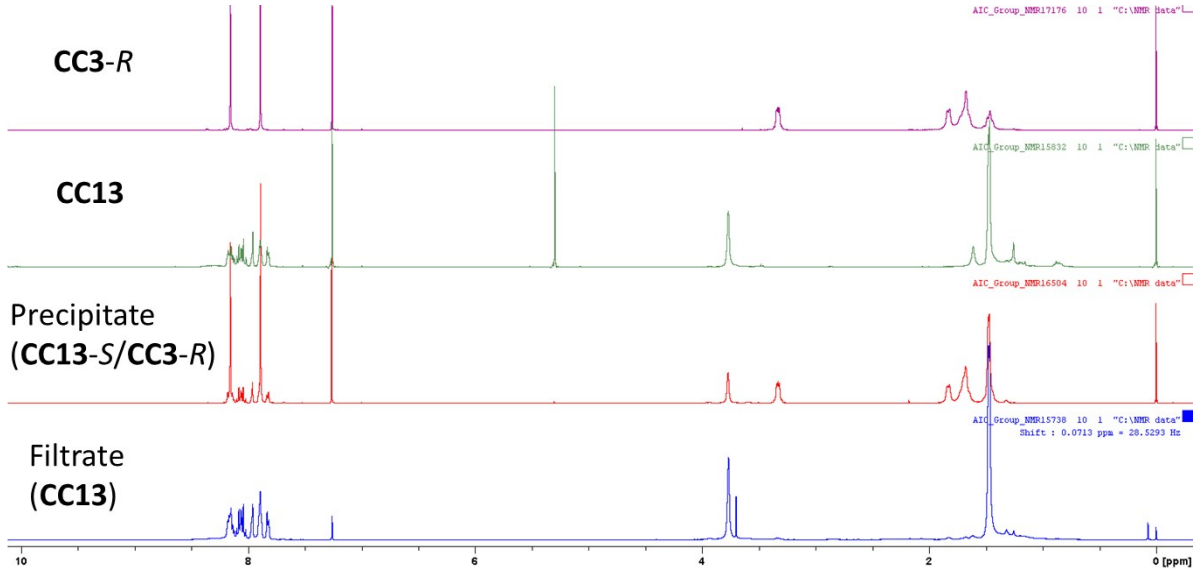

Figure S7: NMR of attempted **CC13** separation by co-crystallisation, and comparison to the pure cages. The precipitate integrates to a 1:0.97 ratio of **CC3** to **CC13**. The filtrate is almost entirely **CC13**.

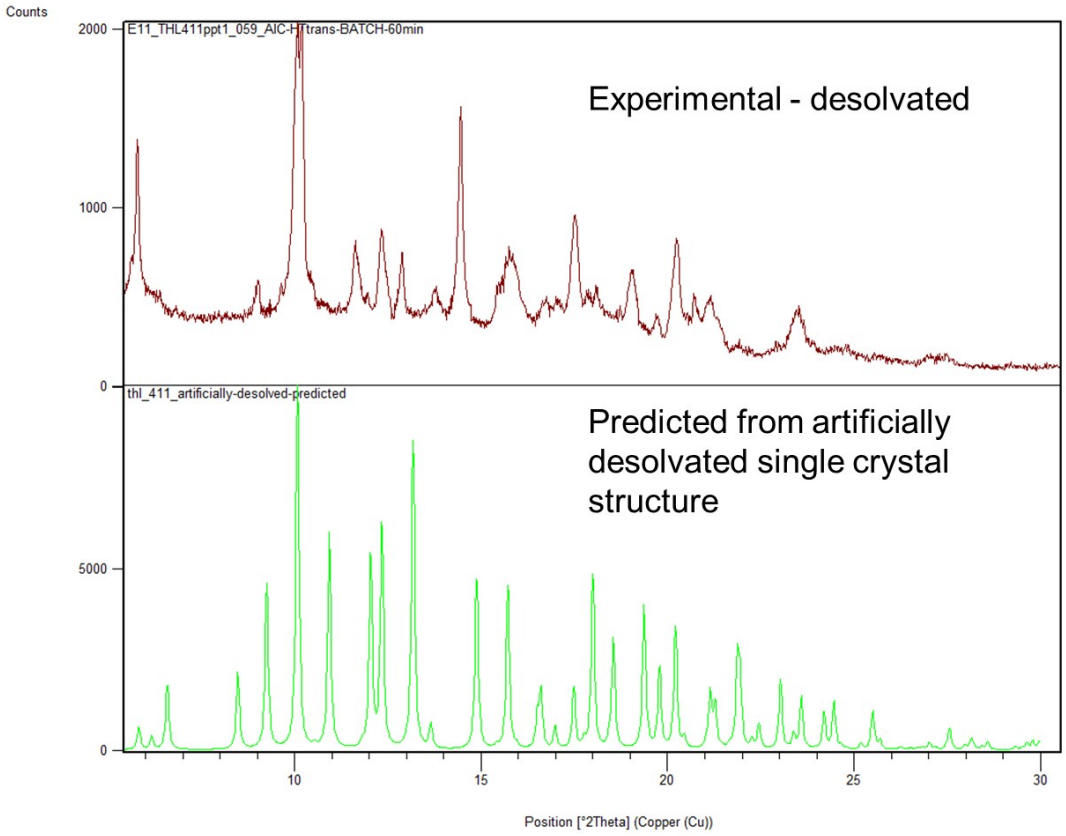

Figure S8: PXRD patterns of **CC3**-*R*/**CC13**-*S* cocrystals grown from DCM/1,4-dioxane. Top: the experimental pattern of the desolvated powder. Bottom: the pattern predicted from the artificially desolvated single crystal structure.

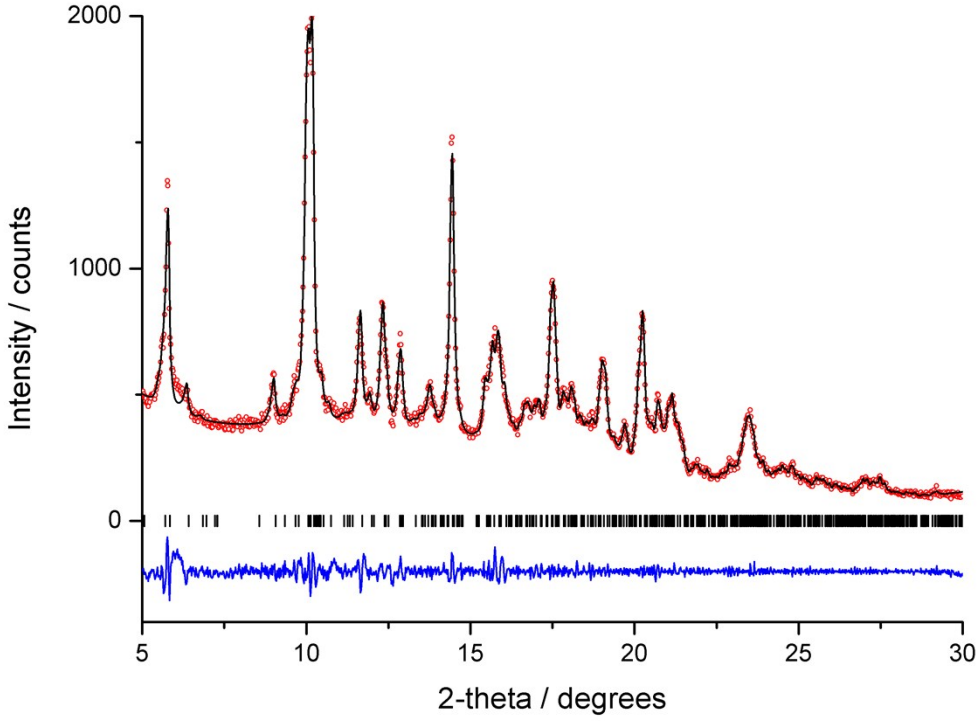

Figure S9: Final observed (red circles), calculated (black line) and difference profiles (blue) for Le Bail refinement (R_{wp} = 4.28 %, R_p = 3.27 %, χ^2 = 2.86) of the **CC3**-*R*/**CC13**-*S* cocrystal (a = 20.681(1), b = 17.039(1), c = 19.706(1) Å, α = 117.531(4), β = 93.950(5) γ = 88.634(5)° V = 6143.0(8) Å^3, P1). The desolvated cell corresponds to a distortion of the single crystal structure from the idealised trigonal geometry, with a significant contraction along the stacking axis (a- and c- axes in the solvent-free and solvate cells, respectively) arising from the removal of solvent between the window-to-window packed **CC3**-**CC13** layers.

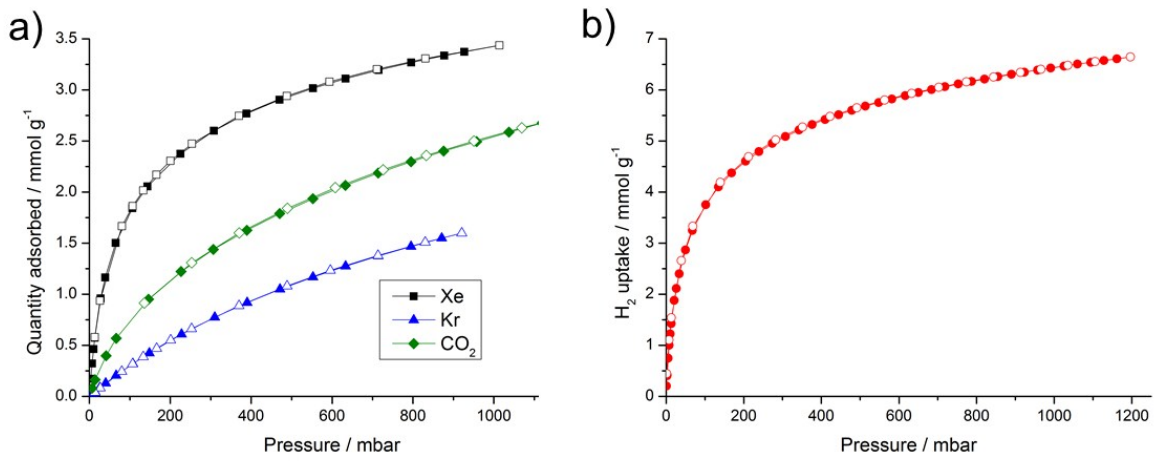

Figure S10: Gas sorption isotherms for cocrystals of **CC3** and **CC13**, in a window-window packing mode. Closed symbols show adsorption and open symbols desorption isotherms. a) Xenon (black squares), krypton (blue triangles) and carbon dioxide (green diamonds), all at 273 K. b) Hydrogen (red circles) at 77 K.

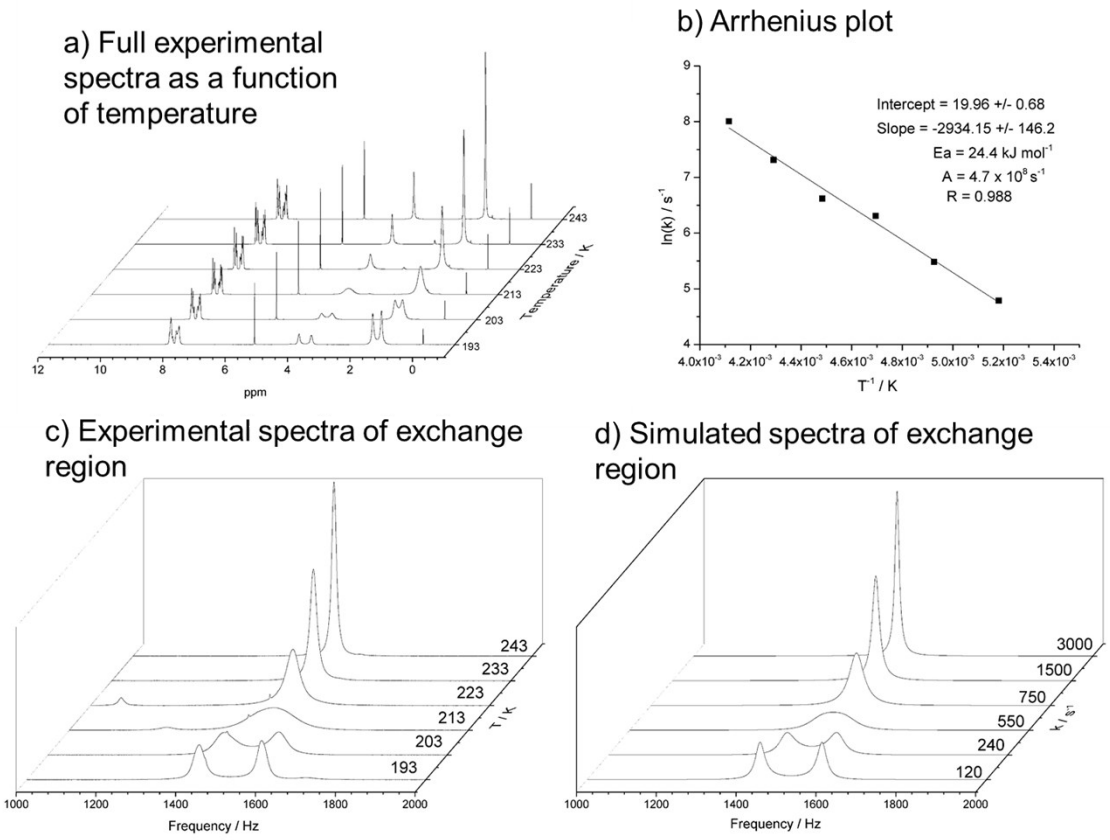

Figure S11: Variable temperature ^{1}H NMR of **CC1$_3$** recorded in CD_2Cl_2. a) Full spectra as a function of temperature. Splitting of the peaks at 3.80 ppm (s, 1 H, N−CH_2-C), and 1.51 ppm (s, 3 H, −$C(CH_3)_2$) can be observed at lower temperatures.; (b) Arrhenius plot using data

obtained in the range 193–243 K; c) Experimental and c) simulated spectra are in good agreement.

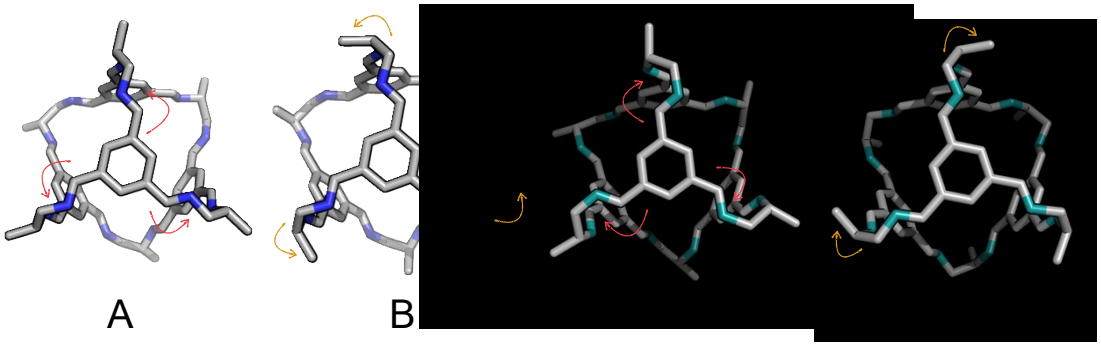

Figure S12: steps involved in the chirality interconversion of **CC2. (**A) is the **CC2**-*R*, the red arrows highlight the orientation of the C-C=N-C torsions before the interconversion. (B) shows the methyl groups – in *exo* position in (A) – moved to the *endo* positions, the process is highlighted by yellow arrows. In (C) all the C-C=N-C torsions are flipped, but with the methyl groups remaining in the *exo* position and in (D) the flipping step and the movement of the methyl groups from *exo* to *endo* are combined. Hydrogens and multiple bonds are omitted for clarity, nitrogens in (C) and (D) are in teal to highlight structural differences from (A) and (B).

Table S1: list of all the modifications applied to **CC1**, **CC2**, **CC3**, and **CC13** to simulate the interconversion mechanism. The "*endo"* keyword stands for the movement of steric bulky groups from the exo to the endo position, the "flip" keyword for the 180 degrees flip of the C-C=N-C torsion. "*1"* is used when only one bulky group was moved and/or when only 1 torsion was flipped, "*All"* when all the bulky groups were moved and/or when all the torsions were flipped.

Cage	Modifications					
CC1		1 flip				
CC2	1 endo	1 flip	1 flip+1 endo	All endo	All flip	All endo+all flip
CC3	1 endo	1 flip	1 flip+1 endo		All flip	
CC13		1 flip				

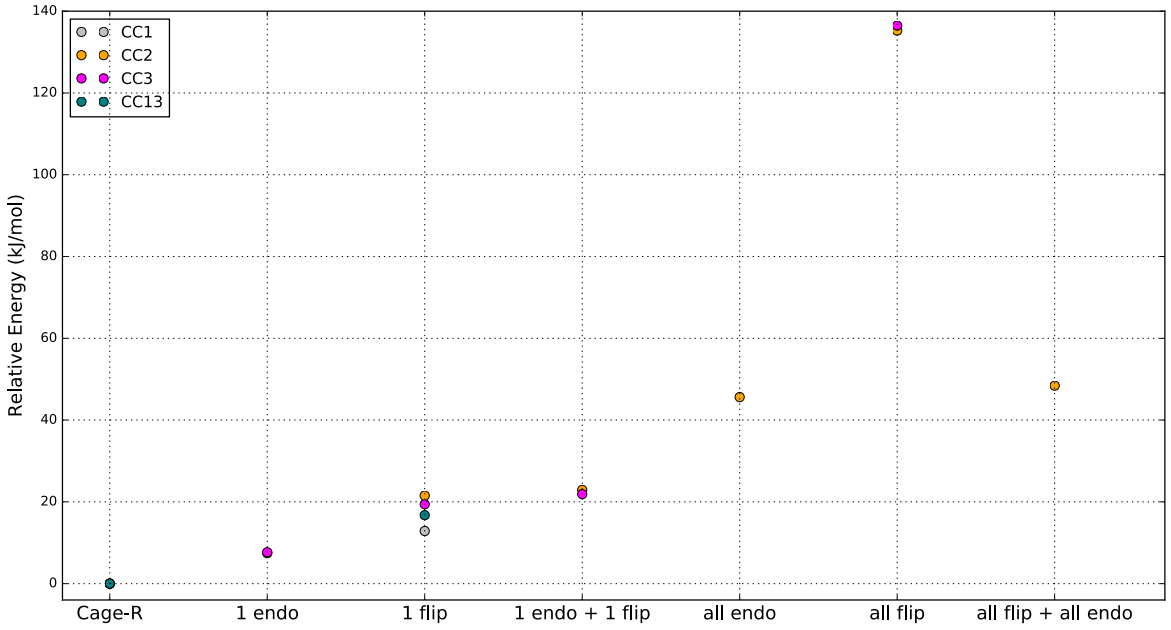

Figure S13: DFT results obtained for CC1, CC2, CC3 and CC13, with the M06-2X functional combined to a 6-31G* basis set. Relative energies are calculated respect to the unmodified Cage-*R*.

References:

1. Hasell, T.; Chong, S. Y.; Jelfs, K. E.; Adams, D. J.; Cooper, A. I., Porous Organic Cage Nanocrystals by Solution Mixing. *Journal of the American Chemical Society* **2012,** *134* (1), 588-598.
2. Hasell, T.; Culshaw, J. L.; Chong, S. Y.; Schmidtmann, M.; Little, M. A.; Jelfs, K. E.; Pyzer-Knapp, E. O.; Shepherd, H.; Adams, D. J.; Day, G. M.; Cooper, A. I., Controlling the Crystallization of Porous Organic Cages: Molecular Analogs of Isoreticular Frameworks Using Shape-Specific Directing Solvents. *Journal of the American Chemical Society* **2014,** *136* (4), 1438-1448.
3. Lydon, D. P.; Campbell, N. L.; Adams, D. J.; Cooper, A. I., Scalable Synthesis for Porous Organic Cages. *Synth. Commun.* **2011,** *41* (14), 2146-2151.
4. Tozawa, T.; Jones, J. T. A.; Swamy, S. I.; Jiang, S.; Adams, D. J.; Shakespeare, S.; Clowes, R.; Bradshaw, D.; Hasell, T.; Chong, S. Y.; Tang, C.; Thompson, S.; Parker, J.; Trewin, A.; Bacsa, J.; Slawin, A. M. Z.; Steiner, A.; Cooper, A. I., Porous organic cages. *Nature Materials* **2009,** *8* (12), 973-978.
5. Nowell, H.; Barnett, S. A.; Christensen, K. E.; Teat, S. J.; Allan, D. R., I19, the small-molecule single-crystal diffraction beamline at Diamond Light Source. *J. Synch. Rad.* **2012,** *19* (3), 435-441.
6. Sheldrick, G. M., SADABS. *University of Göttingen, Germany* **2008**.
7. Sheldrick, G. M., A short history of SHELX. *Acta Cryst. Sect. A* **2008,** *64* (1), 112-122.
8. Dolomanov, O. V.; Bourhis, L. J.; Gildea, R. J.; Howard, J. A. K.; Puschmann, H., OLEX2: a complete structure solution, refinement and analysis program. *J. Appl. Cryst.* **2009,** *42* (2), 339-341.
9. Coelho, A. A. *TOPAS-Academic*, v. 5; Coelho Software, Brisbane, Australia, 2012 http://www.topas-academic.net.
10. Harder, E.; Damm, W.; Maple, J.; Wu, C. J.; Reboul, M.; Xiang, J. Y.; Wang, L. L.; Lupyan, D.; Dahlgren, M. K.; Knight, J. L.; Kaus, J. W.; Cerutti, D. S.; Krilov, G.; Jorgensen, W. L.; Abel, R.; Friesner,

R. A., OPLS3: A Force Field Providing Broad Coverage of Drug-like Small Molecules and Proteins. *Journal of Chemical Theory and Computation* **2016,** *12* (1), 281-296.
11. Santolini, V.; Tribello, G. A.; Jelfs, K. E., Predicting solvent effects on the structure of porous organic molecules. *Chemical Communications* **2015,** *51* (85), 15542-15545.
12. Valiev, M.; Bylaska, E. J.; Govind, N.; Kowalski, K.; Straatsma, T. P.; Van Dam, H. J. J.; Wang, D.; Nieplocha, J.; Apra, E.; Windus, T. L.; de Jong, W., NWChem: A comprehensive and scalable open-source solution for large scale molecular simulations. *Computer Physics Communications* **2010,** *181* (9), 1477-1489.
13. Zhao, Y.; Truhlar, D. G., The M06 suite of density functionals for main group thermochemistry, thermochemical kinetics, noncovalent interactions, excited states, and transition elements: two new functionals and systematic testing of four M06-class functionals and 12 other functionals. *Theoretical Chemistry Accounts* **2008,** *120* (1), 215-241.